Azimuthal anisotropy measurement of (multi-)strange hadrons in Au+Au collisions at $\sqrt{s_{NN}} = 54.4$ GeV

(The STAR Collaboration)

Azimuthal anisotropy of produced particles is one of the most important observables used to access the collective properties of the expanding medium created in relativistic heavy-ion collisions. In this paper, we present second (v_2) and third (v_3) order azimuthal anisotropies of K_S^0, ϕ, Λ, Ξ and Ω at mid-rapidity ($|y| < 1$) in Au+Au collisions at $\sqrt{s_{NN}} = 54.4$ GeV measured by the STAR detector. The v_2 and v_3 are measured as a function of transverse momentum and centrality. Their energy dependence is also studied. v_3 is found to be more sensitive to the change in the center-of-mass energy than v_2. Scaling by constituent quark number is found to hold for v_2 within 10%. This observation could be evidence for the development of partonic collectivity in 54.4 GeV Au+Au collisions. Differences in v_2 and v_3 between baryons and anti-baryons are presented, and ratios of $v_3/v_2^{3/2}$ are studied and motivated by hydrodynamical calculations. The ratio of v_2 of ϕ mesons to that of anti-protons ($v_2(\phi)/v_2(\bar{p})$) shows centrality dependence at low transverse momentum, presumably resulting from the larger effects from hadronic interactions on anti-proton v_2.

I. INTRODUCTION

According to Quantum ChromoDynamics (QCD), at very high temperature (T) and/or large baryonic chemical potential (μ_B) a deconfined phase of quarks and gluons is expected to be present, while at low T and low μ_B quarks and gluons are known to be confined inside hadrons [1]. High energy heavy-ion collisions provide a unique opportunity to study QCD matter at extremely high temperature and density. Experiments at the Relativistic Heavy Ion Collider (RHIC) have shown that a very dense medium of deconfined quarks and gluons is formed in Au+Au collisions at the center-of-mass energy of $\sqrt{s_{NN}} = 200$ GeV [2–9]. Azimuthal anisotropy parameters (v_n), which quantify the azimuthal asymmetries of particle production in momentum space, are an excellent tool to study the properties of the deconfined medium created in these collisions [10–17]. Observations of large v_n magnitudes and their constituent quark scaling in 200 GeV Au+Au collisions ($\mu_B \sim 20$ MeV) have been considered a signature of partonic collectivity of the system [18].

To study the QCD phase structure over a large range in T and μ_B, a beam energy scan program has been carried out by RHIC. The first phase of this program (BES-I) was carried out in 2010-14. Measurements of azimuthal anisotropies of light flavor hadrons made during during the BES-I program by the STAR experiment indicate the formation of QCD matter dominated by hadronic interactions in Au+Au collisions at $\sqrt{s_{NN}} < 11.5$ GeV ($\mu_B > 200$ MeV) [20, 21].

Strange hadrons, especially those containing more than one strange quark, are considered a good probe to study the collective properties of the medium created in high energy heavy-ion collisions, thanks to their early chemical freeze-out and small hadronic interaction cross sections [2, 22–26]. Measurements of (multi-)strange hadron v_n is limited by the available statistics in BES-I. In this paper, we report high precision measurements of azimuthal anisotropy parameters, v_2 and v_3, of strange and multi-strange hadrons at mid-rapidity ($|y| < 1$) in Au+Au col-

lisions at $\sqrt{s_{NN}} = 54.4$ GeV ($\mu_B \sim 90$ MeV). v_2 and v_3 of K_S^0, ϕ, Λ, $\overline{\Xi}$ and Ω are measured as a function of particle transverse momentum (p_T) and collision centrality. Such measurements will provide deep insights into properties of the hot and dense medium, such as partonic collectivity, transport coefficients, and hadronization mechanisms.

This paper is organized in the following manner. In sections II, III and IV, we describe the dataset, the analysis method, and systematic studies respectively. In section V we report the results. Finally, a summary is given in section VI.

II. EXPERIMENTAL SETUP

In this analysis, a total of 600 M minimum bias Au+Au events at $\sqrt{s_{NN}} = 54.4$ GeV recorded by the STAR experiment are used. Events for analysis are selected based on the collision vertex position. Along the beam direction, a vertex position cut of $|V_z| < 30$ cm is applied. A radial vertex position cut (defined as $V_r = \sqrt{V_x^2 + V_y^2}$) of $V_r < 2.0$ cm is used in order to avoid collision with beam pipe whose radius is 3.95 cm.

The trajectory of a charged particle through STAR's magnetic field can be reconstructed, and thus its momentum determined, using the Time Projection Chamber (TPC) [27]. To ensure good track quality, the number of TPC hit points on each track is required to be larger than 15, and the ratio of the number of used TPC hit points to the maximum possible number of hit points along the trajectory should be larger than 0.52. The transverse momentum of each particle is limited to $p_T > 0.15$ GeV/c.

The collision centrality is determined by comparing the uncorrected charged particle multiplicity within a pseudorapidity range of $|\eta| < 0.5$ measured by the TPC with a Glauber Monte Carlo (MC) [28] simulation as shown in Fig. 1. The significant difference between the measured multiplicity and Glauber simulation at low multiplicity
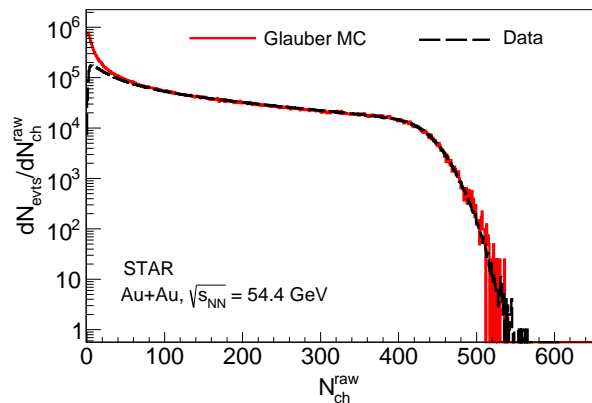
FIG. 1. The uncorrected multiplicity distribution of reconstructed charged particles in Au+Au collisions at $\sqrt{s_{NN}} = $ 54.4 GeV. Glauber Monte Carlo simulation is shown as the solid red curve.

values is due to trigger and primary vertex finding inefficiency. This is corrected by taking the ratio of the simulated multiplicity distribution to that in data as a weight factor. The detailed procedure to obtain the simulated multiplicity distribution using Glauber MC is similar to that described in Ref. [29]. Central (peripheral) events correspond to collisions of large (small) nuclear overlap and thus large (small) charged particle multiplicities.

Particle identification is done using the TPC and the Time-of-Flight (TOF) detectors [30] at mid-pseudorapidity ($|\eta| <$1.0). Both the TPC and TOF have full azimuth coverage. Long-lived charged particles, e.g. π, K, and p, are identified directly using specific ionization energy loss in the TPC and time of flight information in TOF [21]. Short-lived strange hadrons (K_S^0, ϕ, Λ, Ξ, Ω) are reconstructed through two-body hadronic decay channels: $K_S^0 \longrightarrow \pi^+ + \pi^-$, $\phi \longrightarrow K^+ + K^-$, $\Lambda(\bar{\Lambda}) \longrightarrow p(\bar{p}) + \pi^-(\pi^+)$, $\Xi^\pm \longrightarrow \Lambda + \pi^\pm$ and $\Omega^\pm \longrightarrow \Lambda + K^\pm$. K_S^0, Λ, Ξ, and Ω decay weakly and therefore decay topology cuts are applied to reduce the combinatorial background. Cuts on the following topological variables are used: (1) Distance of Closest Approach (DCA) between the two daughter tracks, (2) the DCA of the daughter tracks to the collision vertex, (3) the DCA of the reconstructed parent strange hadron to the collision vertex, (4) the decay length of the strange hadrons, and (5) the angle between the spatial vector pointing from the collision vertex to the decay vertex and the momentum vector of the parent strange hadron. Since the ϕ meson decays strongly, its daughter kaons appear to originate from the collision vertex. The DCAs of kaon tracks from the collision vertex are required to be less than 3 cm for ϕ meson reconstruction.

An event mixing technique is used for the subtraction of combinatorial background for the ϕ mesons [31] and different polynomial functions (1st and 2nd order) are used to fit the background after mixed-event background subtraction. For K_S^0 and Λ, the like-sign method is used

to estimate the background and for Ξ and Ω, the rotational background method is used [32–34]. The invariant mass distributions of K_S^0, ϕ, Λ, Ξ^-, Ω^- and their antiparticles are shown in Fig. 2.

III. ANALYSIS METHOD

The nth order flow coefficient with respect to the event plane is given by

$$v_n = \frac{\langle \cos n(\Phi_i - \psi_n) \rangle}{R_n}, \tag{1}$$

where the angle-bracket represents the average over all the particles in each event and over all the events, Φ_i is the azimuthal angle of the ith particle in an event and ψ_n is the event plane angle for the nth order anisotropy of an event [35]. The R_n denotes the resolution of the nth order event plan angle. The event plane angle can be determined based on the azimuthal distribution of particles in the plane transverse to the collision axis. The nth order event plane angle is given by

$$\psi_n = \frac{1}{n} \tan^{-1} \frac{\sum_i w_i \sin(n\Phi_i)}{\sum_i w_i \cos(n\Phi_i)}. \tag{2}$$

Here w_i is the weight factor taken as p_T of the particle for optimal resolution. The nth order event plane has a symmetry of $2\pi/n$ and one would expect an isotropic distribution of the event plane angle from 0 to $2\pi/n$. However, due to the azimuthally non-uniform detection efficiency of the TPC, the reconstructed event plane angle distribution is usually not isotropic. This is corrected for using the Φ-weight method, details of which can be found in the ref. [35].

To suppress the auto-correlation between particles of interest and those used for event plane angle determination [29, 35], calculations of the v_n coefficients for particles in the positive pseudorapdity region ($0 < \eta < 1$) utilize the sub-event plane determined using particles in the negative pseudorapdity region (-1 $< \eta <$ -0.05), and vice versa. Its definition is the following:

$$v_n = \frac{\langle \cos n(\Phi_i - \psi_n^{A/B}) \rangle}{R_n}, \tag{3}$$

where ψ_n^A and ψ_n^B are the sub-event planes in negative (-1 $< \eta <$ -0.05) and positive (0.05 $< \eta <$1) pseudorapidity regions, respectively. In addition to that, auto-correlation has been removed in the case when decay daughters are distributed in sub-events.
The event plane resolution R_n is estimated using:

$$R_n = \langle \cos n(\psi_n - \psi_R) \rangle = \sqrt{\langle \cos n(\psi_n^A - \psi_n^B) \rangle}, \tag{4}$$

in which ψ_R is the reaction plane angle. Resolution corrections for wide centrality bins are done using the method described in Ref. [36].
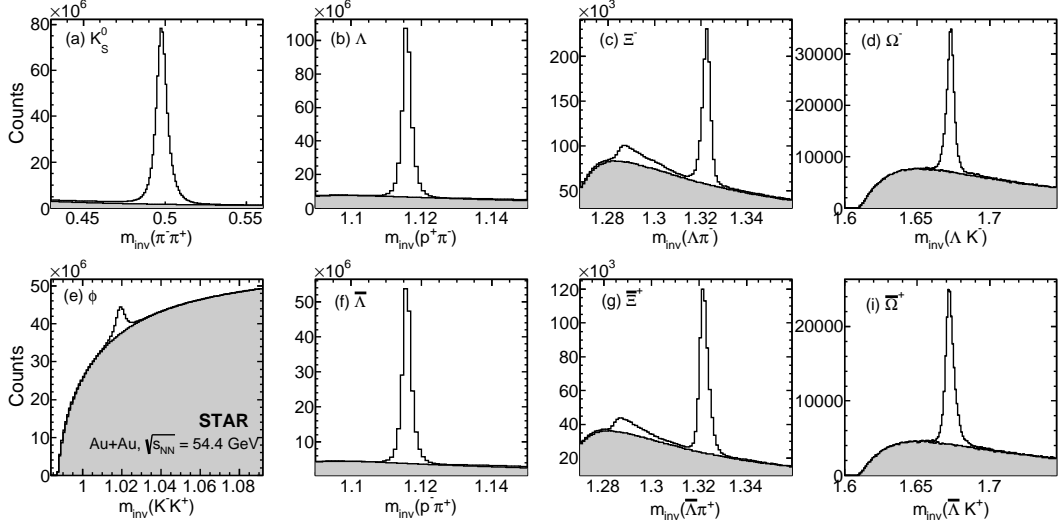
FIG. 2. Invariant mass distributions for K_S^0, ϕ, Λ, Ξ^-, Ω^- and their anti-particles in minimum bias Au+Au collisions at $\sqrt{s_{NN}}$ = 54.4 GeV. The combinatorial background is shown as gray shaded histograms. No background subtraction was included in any of the 8 panels.

By using equation 3, one can calculate the v_n of particles that are detected directly and whose azimuthal distributions are known in every event. But the particles used in this analysis are short-lived and can't be detected directly. To calculate the v_n of such particles, the invariant mass method is used [37], in which the v_n of the particle of interest is calculated as a function of the invariant mass of the decayed daughter particles. Figure 3, taking K_S^0 as an example, shows v_2 and v_3 as a function of the $\pi^+\pi^-$ pair invariant mass in the 10-40% centrality bin. The total v_n of the signal+background can be decomposed into two parts.

$$v_n^{S+B} = v_n^S \frac{S}{S+B} + v_n^B \frac{B}{S+B}. \tag{5}$$

Here v_n^S is the v_n of the signal (K_S^0), v_n^B is the v_n of the background, S is the raw signal counts and B is the background counts. v_n^B is approximated with a first order polynomial function. v_n^S is a free parameter and can be obtained by fitting v_n using Eq. 5, shown as solid red lines in Fig. 3. The v_2 and v_3 of other strange hadrons are calculated in a similar way except for Ξ. For Ξ, Eq. 5 has been modified as follows:

$$v_n^{S+B} = v_n^S \frac{S}{S+B+b} + v_n^b \frac{b}{S+B+b} + v_n^B \frac{B}{S+B+b}, \tag{6}$$

where b denotes the yield of the residual bump observed in the low invariant mass region (see Fig. 2) due to fake Λ candidates [32], and v_n^b denotes the v_n of the residual candidates in the bump region. Systematic checks have been carried out to examine the effect of the bump in Ξ v_n extraction by changing fit ranges and the shape of the background v_n^b at the bump region. The effect is found to be negligibly small, less than 1%, on the v_n values of Ξ particles.
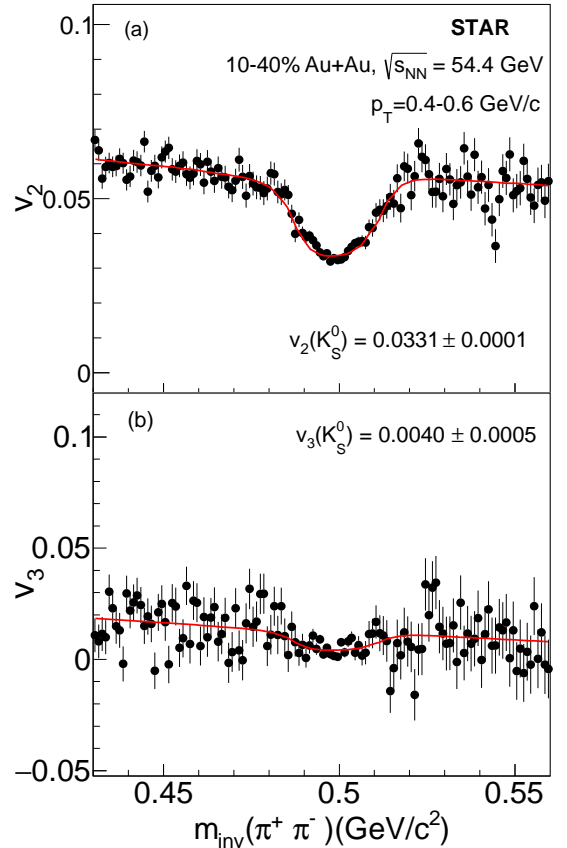

FIG. 3. The upper panel shows v_2 as a function of the invariant mass of $\pi^+\pi^-$ pairs and the lower panel shows the same for v_3. Red lines represent fit functions given in Eq. 5

Particle/Centrality	0-10%	10-40%	40-80%	0-80%
K_S^0	2%	2%	2%	2%
ϕ	10%	3%	3%	5%
Λ	2%	2%	2%	2%
Ξ	4%	3%	3%	3%
Ω	22%	6%	15%	8%

TABLE I. Average systematic uncertainties on v_2 of K_S^0, ϕ, Λ, Ξ and Ω in different centrality bins.

Particle/Centrality	0-10%	10-40%	40-80%	0-80%
K_S^0	3%	3%	3%	3%
ϕ	15%	10%	N.A.	10%
Λ	3%	3%	3%	3%
Ξ	12%	10%	N.A.	8%
Ω	30%	30%	N.A.	30%

TABLE II. Average systematic uncertainties on v_3 of K_S^0, ϕ, Λ, Ξ and Ω in different centrality bins.

IV. SYSTEMATIC UNCERTAINTY

Systematic uncertainties are evaluated by varying event selection cuts, track selection cuts, and background subtraction methods. Track selection cuts used for event plane angle calculation are also varied. For particles like Ξ and Ω the default background construction method is rotational method and for particles like K_S^0 and Λ the default background construction method is the like-sign method. As an alternative to estimate the background fraction, polynomial functions are used to model the residual background in fitting the invariant mass distributions. The resulting differences in v_n between using the default and alternative background estimation methods are included in the systematic uncertainties. For weakly decaying particles, topological cuts are varied as well. Different topological variables are varied simultaneously to keep the raw yield of the particle of interest similar. This helps to reduce the effect of statistical fluctuations in estimating systematic uncertainties. Finally, the Barlow's method [38] is used to determine the systematic uncertainties arising from analysis cut variations. If the resulting changes (Δv_n) in v_n are smaller than the change in statistical errors ($\Delta \sigma_{stat}$) on v_n, such changes are not included in the uncertainties. Otherwise, the systematic error (σ_{sys}) on v_n is calculated as $\sigma_{sys} = \sqrt{(\Delta v_n)^2 - (\Delta \sigma_{stat})^2}$. Finally, systematic uncertainties from different sources, which pass the Barlow check, are added in quadrature. Final systematic uncertainties are calculated as a function of p_T and centrality. They are found to be nearly p_T independent but larger in central collisions compared to peripheral collisions. Table I and II show the average systematic uncertainties on v_2 and v_3 for K_S^0, ϕ, Λ, Ξ and Ω in different centrality bins.

V. RESULTS AND DISCUSSION

A. p_T dependence of v_2 and v_3

The transverse momentum dependence of v_2 and v_3 for K_S^0, ϕ, Λ, Ξ^-, Ω^- (and their anti-particles) is shown in Fig. 4. The measurements are done at mid-rapidity, $|y| < 1.0$, in minimum bias Au+Au collisions at $\sqrt{s_{NN}}$ = 54.4 GeV. The non-zero magnitude of v_3 is consistent with the picture of event-by-event fluctuations in the initial density profile of the colliding nuclei [39]. Both v_2 and v_3 initially increase with p_T and then tend to saturate. This may be due to the interplay of hydrodynamic flow as well as viscous effects [40]. The magnitude of v_3 is found to be less than that of v_2 for all particles in 0-80% centrality. This is the first v_3 measurement of the multi-strange baryons Ξ and Ω in relativistic heavy-ion collisions. The v_n of heavy multi-strange baryons like Ω are similar to that of the lighter mass, strange baryon Λ. The v_n of ϕ mesons, which consist of strange and anti-strange quark pairs, is similar to that of light, strange K_S^0. If v_n is developed through hadronic interactions, v_n should depend on the cross-sections of the interacting hadrons and therefore those (e.g. ϕ, Ω) with smaller cross-sections should develop less momentum anisotropy. Therefore the observed large v_n of ϕ and Ω are consistent with the scenario that the anisotropy is developed in the partonic medium in Au+Au collisions at $\sqrt{s_{NN}}$ = 54.4 GeV. We also observe a difference in v_n between baryon and anti-baryon which is discussed separately in a later section. The high precision measurements of v_n for K_S^0, ϕ, Λ, Ξ, and Ω presented in this paper can be used to constrain various models, for example, in extracting transport properties of the medium created at $\sqrt{s_{NN}}$ = 54.4 GeV.

B. Centrality dependence of v_2 and v_3

The centrality dependence of v_2 and v_3 of K_S^0, ϕ, Λ, Ξ^-, Ω^- (and their anti-particles) are studied. Figures 5 and 6 show v_2 and v_3, respectively, as a function of p_T for three different centrality classes, 0-10%, 10-40% and 40-80%. For ϕ, Ξ and Ω measurements are only possible for v_3 for the 0-10% and 10-40% centralities due to data sample size. We observe a strong centrality dependence of v_2 for all the particles, with the magnitude increasing from central to peripheral collisions. This is expected if v_2 is driven by the shape of the initial overlap of the two colliding nuclei [29].

We observe a weak centrality dependence for v_3 compared to v_2. This observation is consistent with the scenario in which v_3 mostly originates from event-by-event fluctuations of participant nucleon distributions [39], instead of the impact parameter dominated average participant anisotropy distributions. Our measurements demonstrate that such scenario also works well for 54.4 GeV Au+Au collisions.
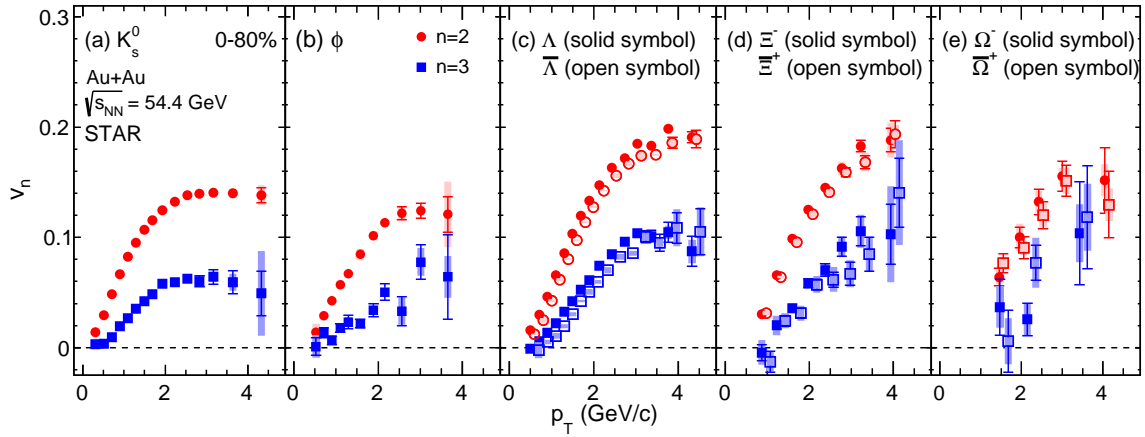
FIG. 4. v_2 and v_3 as a function of p_T at mid-rapidity($|y| < 1$) for minimum bias events. The vertical lines represent the statistical error bars and the shaded bands represent the systematic uncertainties. Data points for anti-particles are shifted by 0.1 GeV/c towards right for better visibility.
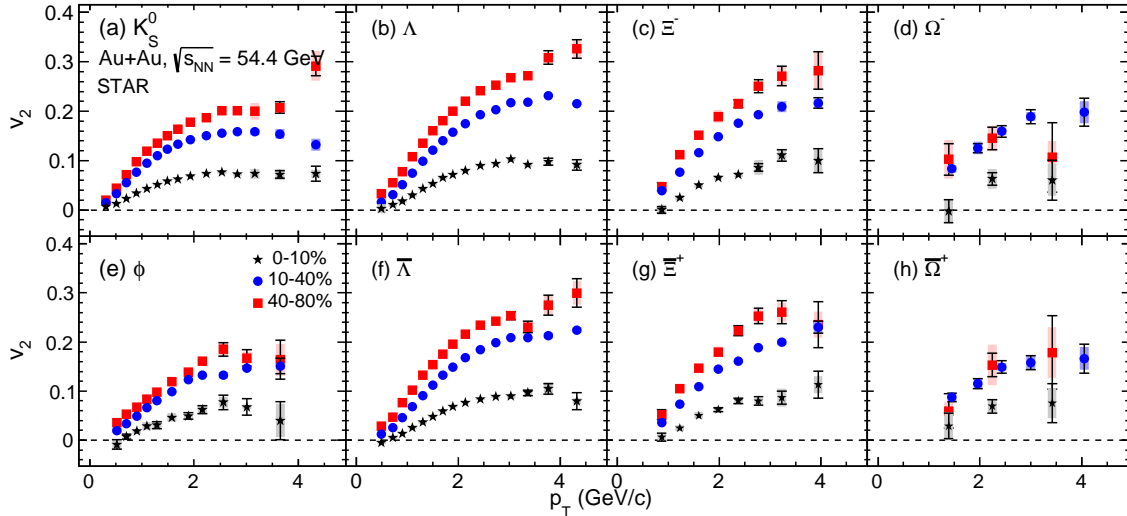

FIG. 5. v_2 as function of p_T for 0-10%, 10-40% and 40-80% centrality events. The vertical lines represent the statistical error bars and the shaded bands represent the systematic uncertainties.

C.   Energy dependence of v_2 and v_3

The high statistics data at 54.4 GeV from the STAR experiment offer an opportunity to study the collision energy dependence of v_2 and v_3 of strange hadrons. Figure 7 upper panels show v_2 of K_S^0, ϕ, $\bar{\Lambda}$, $\bar{\Xi}^+$, and Ω^- as a function of p_T in 0-80% centrality at $\sqrt{s_{NN}} = 39$, 54.4, and 200 GeV. Lower panels show the ratios with polynomial fits to the 200 GeV data points. K_S^0 v_2 at 54.4 GeV is smaller than at 200 GeV, and higher than at 39 GeV. The maximum difference is at intermediate p_T. For $\bar{\Lambda}$ and $\bar{\Xi}^+$, v_2 at 54.4 GeV (as well as at 39 GeV) is higher than at 200 GeV at very low p_T. This could be due to the effect of large radial flow at 200 GeV compared to 54.4 and 39 GeV. This effect is only visible in heavier hadrons like $\bar{\Lambda}$ and $\bar{\Xi}^+$. For ϕ and Ω^-, statistical errors at low

p_T are too large to draw any conclusions. Figure 8 upper panels shows v_3 of K_S^0, ϕ, and $\bar{\Lambda}$ as a function of p_T in 0-80% centrality at $\sqrt{s_{NN}} = 54.4$, and 200 GeV. Lower panels show the ratios of fits to the 200 GeV data points. We observe that the difference in v_3 between 54.4 and 200 GeV is almost p_T independent for all the particles studied. In Fig. 8, the v_3 shows greater variation as a function of beam energy than that of v_2. The measured ratio of $v_3(54.4 \text{ GeV})/v_3(200 \text{ GeV})$ for K_S^0 is ~0.8 while the same ratio for v_2 is approaching 0.9. This suggests that the dynamics responsible for v_3, presumably fluctuations dominated, are more sensitive to beam energy than the v_2.
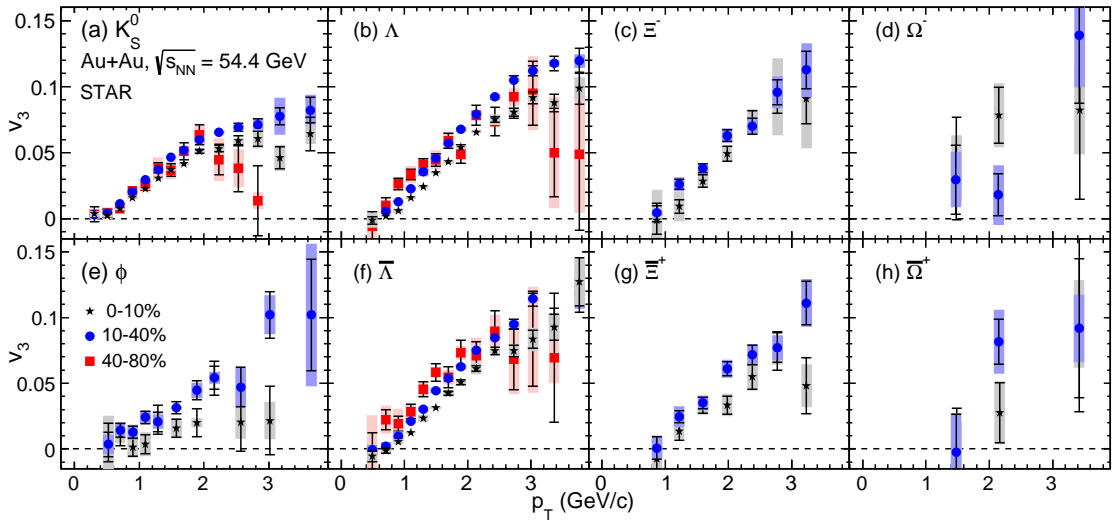
FIG. 6. v_3 as function of p_T for 0-10%, 10-40% and 40-80% centrality events. The vertical lines represent the statistical error bars and the shaded bands represent the systematic uncertainties. 40-80% centrality data points are not shown for Ξ and Ω due to less statistics.
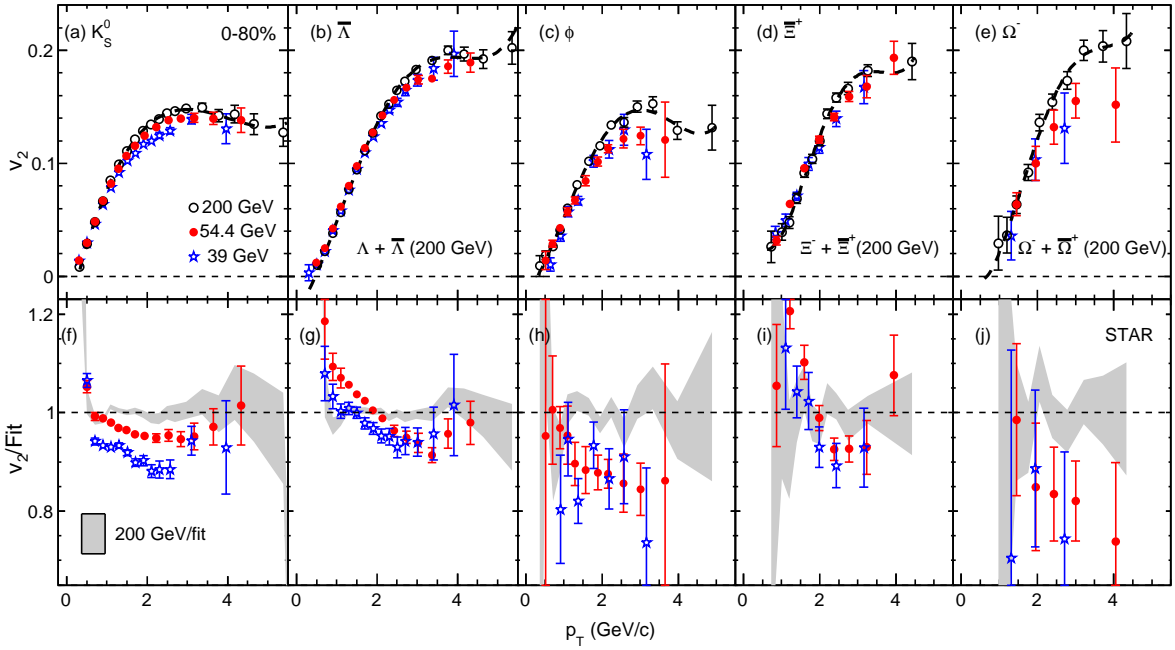

FIG. 7. v_2 of K_S^0, ϕ, $\bar{\Lambda}$, $\bar{\Xi}^+$, and Ω^- as a function of p_T in 0-80% centrality events at $\sqrt{s_{\mathrm{NN}}} = 39$, 54.4, and 200 GeV. The dotted line represents the fit to the 200 GeV data points. The vertical lines represent the sum of statistical and systematic uncertainties in quadrature. The data points for 39 and 200 GeV are taken from refs. [18, 20, 41]

D. v_n of particles and anti-particles

In the upper panels Fig 9, we show the ratio of v_2 and v_3 of particles ($v_n(X)$) to the corresponding anti-particles ($v_n(\bar{X})$) for Λ, Ξ, and Ω in 10-40% centrality as a function of p_T. We also present the difference between v_2 and v_3 of particles and anti-particles in the lower panels of Fig . 9. We can not establish a clear p_T depen-dence in the ratio or difference of multi-strange parti-cle and anti-particle. The Λ and $\bar{\Lambda}$ v_n data seem to be consistent with a relatively smaller v_n for $\bar{\Lambda}$ in the low p_T region. We have calculated the p_T integrated aver-age difference in v_n between baryon and anti-baryon by fitting the $v_n(X) - v_n(\bar{X})$ versus p_T with a zeroth or-der polynomial function as done in Ref. [20]. Figure 10 shows the average difference between v_n of baryons and
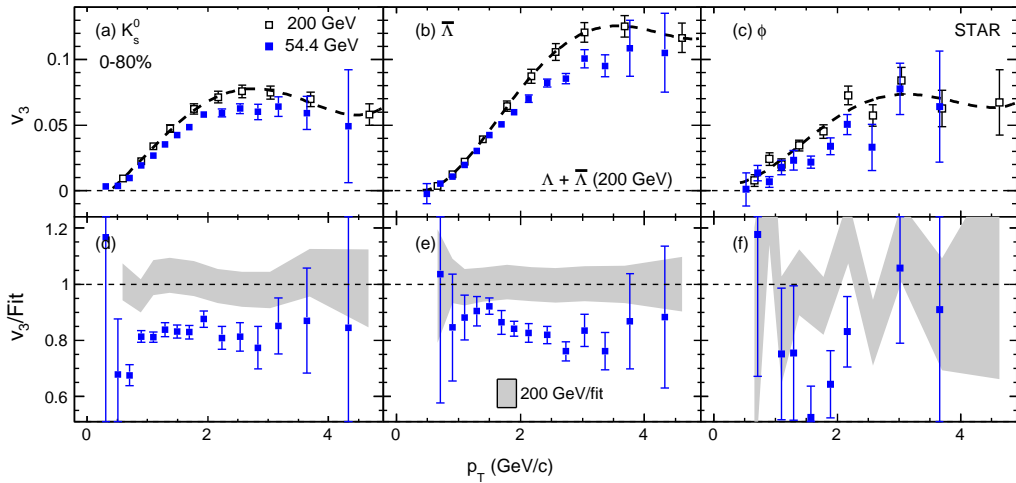
FIG. 8. v_3 of K_S^0, ϕ and $\bar{\Lambda}$ as a function of p_T in 0-80% centrality events at $\sqrt{s_{NN}} = 54.4$, and 200 GeV. The vertical lines represent the sum of statistical and systematic uncertainties in quadrature. The data points for 200 GeV are taken from ref. [42].

anti-baryons for Λ, Ξ, and Ω in 10-40% centrality as a function of mass. The difference is independent of baryon species within the measured uncertainty for both v_2 and v_3. The magnitude of the observed difference between particle and anti-particle is similar to that in 62.4 GeV published by the STAR experiment [21]. However, uncertainties on the measured values are significantly reduced at 54.4 GeV. The observed difference between particles and anti-particles could arise due to the effect of transported quarks at low beam energies as predicted in [43]. Alternatively, a calculation based on the Nambu-Jona-Lasinio (NJL) model [44, 45] can also qualitatively explain the differences between particles and anti-particles by considering the effect of the vector mean-field potential, which is repulsive for quarks and attractive for anti-quarks. We also measure the difference between Ω^- and $\bar{\Omega}^+$, however the observed difference is not statistically significant ($<1\sigma$ significance).

E. $v_3/v_2^{3/2}$ ratio

The ratios between different orders of flow harmonics are predicted to be sensitive probes of transport properties of the produced medium in heavy-ion collisions. According to hydrodynamic model calculations, the ratio $v_3/v_2^{3/2}$ is independent of p_T and its magnitude depends on the properties of transport properties (e.g., viscosity) of the medium [46–48]. We have calculated the ratio $v_3/v_2^{3/2}$ as a function of p_T for K_S^0, Λ, Ξ^-, Ω^-, ϕ, $\bar{\Lambda}$, $\bar{\Xi}^+$ and $\bar{\Omega}^+$ for 10-40% centrality, as shown in Fig. 11. Our measurement for K_S^0 clearly demonstrates a p_T dependence of the ratio. The p_T dependence of the ratios for Λ is weak and ratios for other strange hadrons are limited by statistical errors. Detailed comparisons with other RHIC measurements [49, 50] and with more hy-

drodynamic model calculations will shed more light on the dynamics.

F. Number of constituent quark scaling of v_2 and v_3

Elliptic flow measurements at top RHIC energy suggest that a strongly-interacting partonic matter is produced in Au+Au collisions [18]. This conclusion is based in part on the observation that the elliptic flow for identified baryons and mesons when divided by the number of constituent quarks (n_q) is found to scale with the transverse kinetic energy of the particles.

Figure 12(a) and (b) show the v_2/n_q as a function of n_q scaled transverse kinetic energy in 10-40% central Au+Au collisions at $\sqrt{s_{NN}} = 54.4$ GeV. The transverse kinetic energy is m_T-m_0 where m_T is the transverse mass given by $m_T = \sqrt{m_0^2 + p_T^2}$ and m_0 is the rest mass of the particle. Due to the observed difference in particle and anti-particle v_n we plot v_2/n_q vs. $(m_T$-$m_0)/n_q$ for particle and anti-particle separately. The n_q-scaled v_2 for identified hadrons including multi-strange hadrons are found to scale with the scaled kinetic energy of the particles. To quantify the validity of scaling we have fitted the scaled v_2 of K_S^0 with a 4th order polynomial, and ratios to the fit for different particles have shown in lower panels of Fig. 12. It is found that the scaling holds within a maximum deviation of 10% for all the particles. The observed scaling in v_2 can be interpreted as due to the development of substantial collectivity in the partonic phase [51] and as evidence that coalescence is the dominant mechanism of particle production for the intermediate p_T range.

The scaling properties in v_3 have also been examined by plotting $v_3/(n_q)^{3/2}$ as a function of $(m_T$-$m_0)/n_q$ as shown in panels (a) and (b) of Fig. 13. From the ratios shown in the lower panels, we note that the scaling of
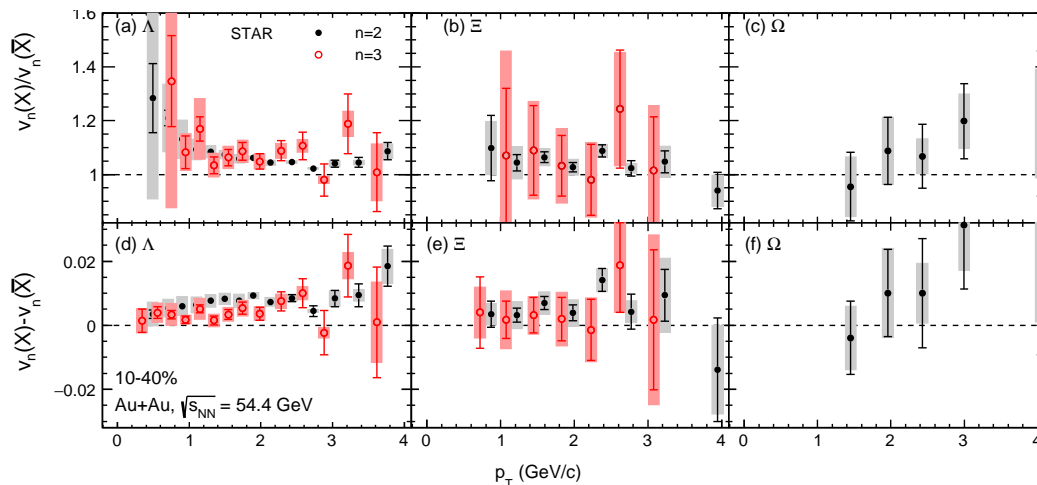
FIG. 9. Three upper panels, a, b, and c show the ratio of v_n of particles to anti-particles for Λ, Ξ and Ω respectively in 10-40% centrality. The lower panels show the difference between v_n of particles to anti-particles. The vertical lines represent the statistical error bars and the shaded bands represent the systematic uncertainties. Data points for v_3 are shifted by 0.15 GeV/c towards the left for better visibility. For the Ω, data points for v_3 were not shown due to fewer statistics.
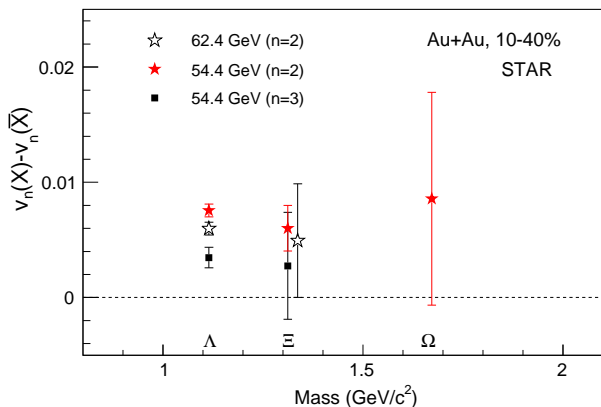
FIG. 10. The difference of v_n of particles and anti-particles is plotted as a function of mass. The result is compared with 62.4 GeV. Uncertainties represent the sum of statistical and systematic in quadrature.

$v_3/(n_q)^{3/2}$ is clearly violated for Λ particles and the statistical errors for multi-strange particles are too large to draw a conclusion regarding scaling.

G. $\quad v_2(\phi)/v_2(\bar{p})$ ratio

Among many mesons, the $\phi(s\bar{s})$ has unique properties. It has a mass of 1.019 GeV/c^2 which is comparable to the mass of the lightest baryon, the proton (0.938 GeV/c^2). The hadronic interaction cross-section of the ϕ is expected to be small compared to ordinary hadrons consisting of up and down quarks such as the proton (uud). Therefore, the kinematic properties of ϕ are expected to be less affected by the later stage hadronic interactions compared to the proton.

Hydrodynamical model calculations predict that v_2 of identified hadrons as a function of p_T will follow mass ordering, where the v_2 of lighter hadrons is higher than that of heavier hadrons. A phenomenological calculation [52], based on ideal hydrodynamics together with a hadron cascade (JAM), shows that because of late-stage hadronic rescattering effects on the proton, the mass ordering in v_2 will be violated between ϕ and proton at very low p_T. This model calculation was done by assuming a small hadronic interaction cross-section for the ϕ meson and a larger hadronic interaction cross-section for proton. The breaking of mass ordering in v_2 between ϕ and proton was observed in central Au+Au collisions at $\sqrt{s_{NN}} = 200$ GeV and reported by the STAR experiment in Ref. [18].

Figure 14(a) shows $v_2(\phi)/v_2(\bar{p})$ vs. p_T for 10-40% and 40-80% centralities at $\sqrt{s_{NN}} = 54.4$ GeV. The result for 0-10% is not shown due to very large uncertainties. Anti-protons, which consist of all produced quarks ($\bar{u}\bar{u}\bar{d}$), are used instead of protons to avoid the effect of transported quarks. At $p_T = 0.5$ GeV/c, the ratio is greater than one with 1σ significance in 10-40% centrality. In addition, $v_2(\phi)/v_2(\bar{p})$ ratios in 10-40% central collisions are found to be systematically higher than in peripheral 40-80% events. This observed centrality dependence could be the result of more hadronic rescattering effect on v_2 of $\bar{p}$ compared to ϕ, since ϕ mesons have small hadronic interaction cross-section [22, 53]. Comparison of the ratios for 0-80% collision centrality from $\sqrt{s_{NN}} = 54.4$ GeV and 200 GeV shows consistency with each other within uncertainties for $p_T < 1.0$ GeV/c.
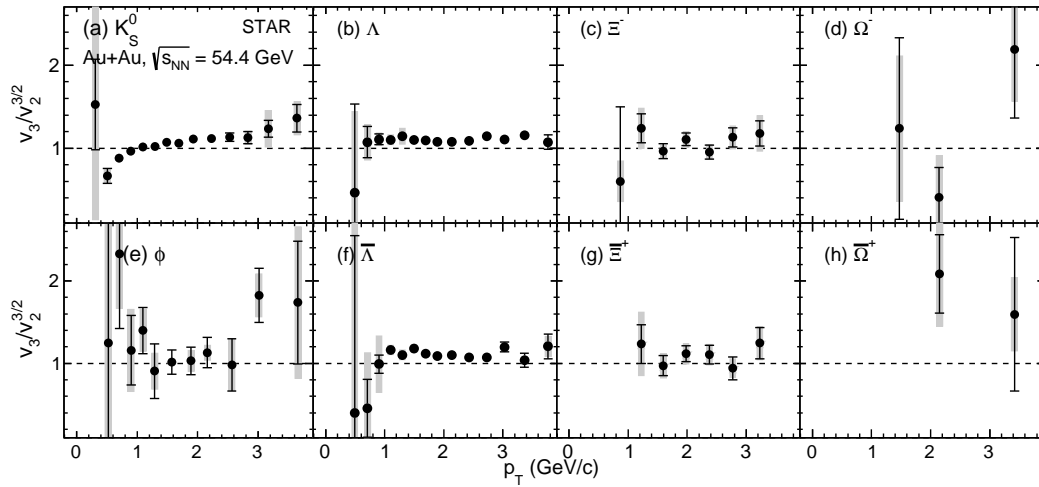
FIG. 11. $v_3/v_2^{3/2}$ is plotted as a function of p_T for K_S^0, Λ, Ξ^-, Ω^-, ϕ, $\bar{\Lambda}$, $\bar{\Xi}^+$ and $\bar{\Omega}^+$ in 10-40% central Au+Au collisions at $\sqrt{s_{NN}} = 54.4$ GeV.

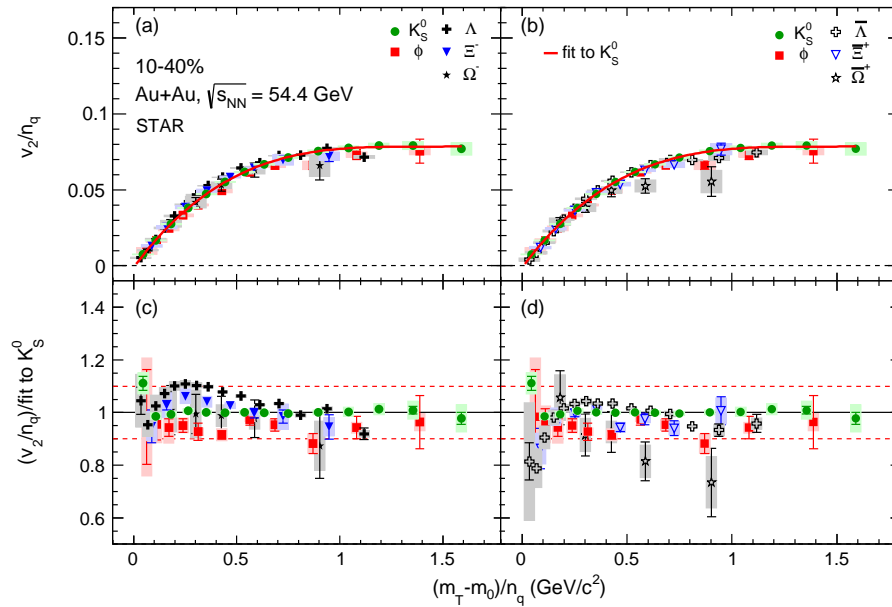FIG. 12. Panel (a) shows the n_q-scaled v_2 as a function of n_q-scaled transverse kinetic energy for K_S^0, ϕ, Λ, Ξ^- and Ω^- in 10-40% centrality class events. Panel (b) shows the same for K_S^0, ϕ, $\bar{\Lambda}$, $\bar{\Xi}^+$ and $\bar{\Omega}^+$. The red line shows the polynomial fit to the K_S^0 data points. Panels (c) and (d) show the ratio of n_q-scaled v_2 of all the particles to the fit function.

VI. SUMMARY

In summary, we have reported the azimuthal anisotropic flow parameters, v_2 and v_3, of strange and multi-strange hadrons, K_S^0, ϕ, Λ, Ξ^-, Ω^- (and their anti-particles) measured at mid-rapidity as a function of p_T for various collision centralities in Au+Au collisions at $\sqrt{s_{NN}} = 54.4$ GeV. The magnitude of v_3 of multi-strange baryons Ξ and Ω is found to be similar to that of the lighter strange baryon Λ. The non-zero magnitude of v_3 indicates the presence of event-by-event fluctuations in the initial energy density profile of colliding nuclei and

large values of v_2 and v_3 of multi-strange hadrons indicate that the observed collectivity is mainly developed through partonic rather than hadronic interactions.

The centrality dependence of v_3 is weak relative to that of v_2 which is consistent with the scenario that v_3 does not arise from impact parameter driven average spatial configurations, rather it originates dominantly from event-by-event fluctuation present in the system. The measured v_2 and v_3 values at $\sqrt{s_{NN}} = 54.4$ GeV are also compared with available published results in Au+Au collisions at $\sqrt{s_{NN}} = 39$ and 200 GeV to examine the energy dependence. We observed that the change in v_3 with
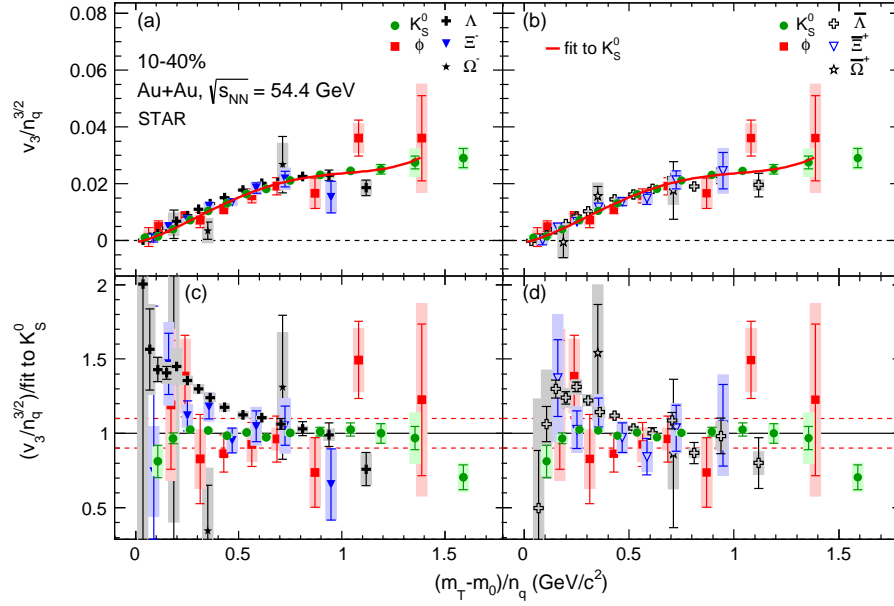
FIG. 13. Panel (a) shows $v_3/n_q^{3/2}$ as a function of n_q-scaled transverse kinetic energy for K_S^0, ϕ, Λ, Ξ^- and Ω^- in 10-40% centrality class events. Panel (b) shows the same for K_S^0, ϕ, $\bar{\Lambda}$, $\bar{\Xi}^+$ and $\bar{\Omega}^+$. The red line shows the polynomial fit to the K_S^0 data points. Panels (c) and (d) show the ratio of $v_3/n_q^{3/2}$ of all the particles to the fit function.
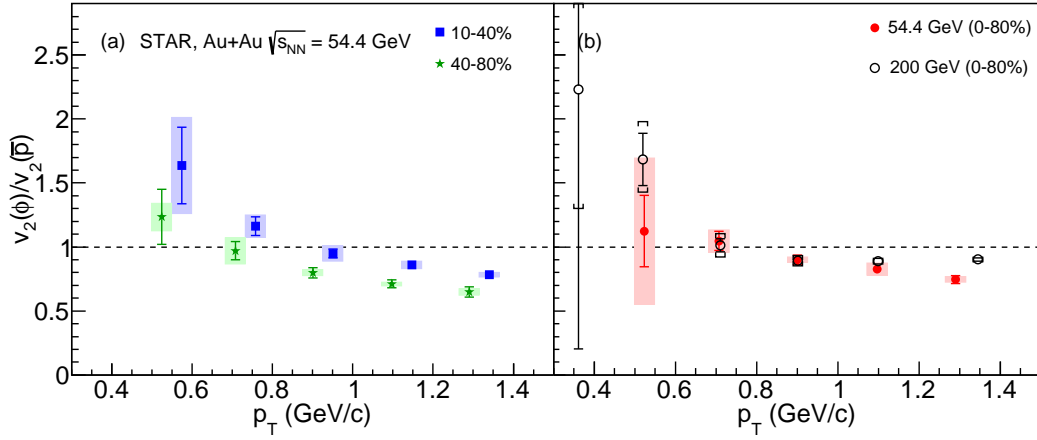

FIG. 14. Left panel shows the ratio of v_2 of ϕ to v_2 of $\bar{p}$ as a function of p_T for 10-40% and 40-80% centralities at $\sqrt{s_{NN}}$ = 54.4 GeV. Data points for 10-40% centrality are shifted by 0.05 GeV/c to the right for better visibility. The right panel shows the comparison of the ratio at $\sqrt{s_{NN}}$ = 54.4 GeV and 200 GeV in 0-80% centrality. For 200 GeV [18], the measured ratio is $v_2(\phi)/v_2(p + \bar{p})$. The vertical lines represent the statistical error bars and the shaded bands represent the systematic uncertainties. Data points at 200 GeV are taken from ref. [18]

$\sqrt{s_{NN}}$ is more than that in v_2. This suggests that v_3 dynamics have stronger energy dependence compared to v_2. A difference in $v_n(p_T)$ between baryons and corresponding antibaryons was observed. The observed difference is found to be baryon-type independent within uncertainties.

We have studied the n_q scaling for both v_2 and v_3 and found that the scaling holds for v_2 of all the particles while the scaling for v_3 seems to be violated. One interpretation of the observed n_q scaling in v_2 is that

parton recombination is the dominant mechanism for hadronization at mid-rapidity and the development of collectivity occurs during the partonic stage of the system evolution. The ratio $v_3/v_2^{3/2}$, which is sensitive to the medium properties according to hydrodynamic calculations, shows weak p_T dependence for $p_T > 1$ GeV/c, similar to the behaviour of this ratio was found in the previous study with U+U collisions at 193 GeV. The $v_2(\phi)/v_2(\bar{p})$ ratio was presented as a function of p_T for two different centrality classes 10-40% and 40-80%. The

$v_2(\phi)/v_2(\bar{p})$ ratio shows a decreasing trend as a function of p_T for both collision centralities. The $v_2(\phi)/v_2(\bar{p})$ ratio is also found to be systematically higher for central collisions 10-40% than non-central collisions 40-80%. This could be due the effect of more hadronic rescattering on v_2 of $\bar{p}$ compared to ϕ and hence our measurements are consistent with the picture of a small hadronic cross-section of the ϕ meson.

ACKNOWLEDGMENTS

[1] D. J. Gross, R. D. Pisarski, and L. G. Yaffe, Rev. Mod. Phys. 53, 43 (1981).
[2] J. Adams *et al.*, (STAR Collaboration) Nucl. Phys. A757, 102 (2005).
[3] K. H. Ackermann *et al.*, (STAR Collaboration), Phys. Rev. Lett. 86, 402 (2001).
[4] J. Adams *et al.*, (STAR Collaboration), Phys. Rev. Lett. 92, 052302 (2004).
[5] J. Adams *et al.*, (STAR Collaboration), Phys. Rev. C 72, 014904 (2005).
[6] B. I. Abelev *et al.*, (STAR Collaboration), Phys. Rev. Lett. 99,112301 (2007).
[7] S. S. Adler *et al.*, (PHENIX Collaboration), Phys. Rev. Lett. 91, 182301 (2003).
[8] S. S. Adler *et al.*, (PHENIX Collaboration), Phys. Rev. Lett. 94, 232302 (2005).
[9] B. Alver *et al.* (PHOBOS Collaboration), Phys. Rev. Lett. 98, 242302 (2007).
[10] J. Y. Ollitrault, Phys. Rev. D 46, 229 (1992).
[11] P. Huovinen, P. F. Kolb, U. Heinz, P. V. Ruuskanen, and S.A. Voloshin *et al.*, Phys. Lett. B 503, 58 (2001).
[12] C. Shen and U. Heinz, Phys. Rev. C 85, 054902 (2012).
[13] R. Snellings, New J. Phys. 13, 055008 (2011).
[14] H. Appelshauser *et al.*, (NA49 Collaboration), Phys. Rev. Lett. 80, 4136 (1998).
[15] K. Aamodt *et al.*, (ALICE Collaboration), Phys. Rev. Lett. 105, 252302 (2010).
[16] G. Aad *et al.*, (ATLAS Collaboration), Phys. Lett. B 707, 330 (2012).
[17] S. Chatrchyan *et al.* (CMS Collaboration), Phys. Rev. C 89, 044906 (2014)
[18] L. Adamczyk *et al.*, (STAR Collaboration), Phys. Rev. Lett. 116, 062301 (2016).
[19] M.M. Aggarwal *et al.*, (STAR Collaboration), arXiv:1007.2613.
[20] L. Adamczyk *et al.*, (STAR Collaboration) Phys. Rev. Lett. 110, 142301 (2013).
[21] L. Adamczyk *et al.*, (STAR Collaboration) Phys. Rev. C 88, 014902 (2013).
[22] A. Shor, Phys. Rev. Lett. 54, 1122 (1985).
[23] X. Luo, et al. Particles 3, no.2, 278 (2020).
[24] B. Mohanty and N. Xu, J. Phys. G 36, 064022 (2009).
[25] J.H. Chen, et al., Phys. Rev. C 74, 064902 (2006).
[26] M. Nasim, B. Mohanty, and N. Xu, Phys. Rev. C 87, 014903 (2013).
[27] K.H. Ackermann et al., Nucl. Instrum. Methods Phys. Res., Sect. A 499, 624 (2003).
[28] R. J. Glauber, Nucl. Phys. A 774, 3 (2006).
[29] L. Adamczyk *et al.*, (STAR Collaboration) Phys. Rev. C 86, 054908 (2012).
[30] W. J. Llope (STAR TOF Group), Nucl. Instrum. Methods Phys.Res., Sect. B 241, 306 (2005).
[31] D. Drijard, H.G. Fischer and T. Nakada, Nucl. Inst. Meth. in Phys. Res. A 225, 367 (1984).
[32] J. Adams *et al.*, (STAR Collaboration) Phys. Rev. Lett. 95, 122301 (2005).
[33] C. Adler *et al.*, (STAR Collaboration) Phys. Rev. Lett. 89, 132301 (2002).
[34] M. S. Abdallah *et al.*, (STAR Collaboration) Phys. Rev. C 103, 064907, (2021).
[35] A. M. Poskanzer and S. A. Voloshin, Phys. Rev. C 58, 1671 (1998).
[36] H. Masui, A. Schmah, A. M. Poskanzer, Nucl. Instrum. Meth. A833, 181 (2016).
[37] N. Borghini and J.-Y. Ollitrault, Phys. Rev. C 70, 064905 (2004).
[38] R. Barlow, arXiv:hep-ex/0207026.
[39] B. Alver and G. Roland, Phys. Rev. C 81, 054905 (2010); 82, 039903(E) (2010);
[40] M. Luzum, P. Romatschke, Phys. Rev. C 78, 034915 (2008).
[41] B. I. Abelev *et al.*, (STAR Collaboration) Phys. Rev. C 77, 054901 (2008).
[42] M. S. Abdallah *et al.*, (STAR Collaboration) arXiv:nucl-ex/2203.07204
[43] J. C. Dunlop, M. A. Lisa, and P. Sorensen, Phys. Rev. C 84, 044914 (2011).
[44] C. M. Ko *et al.*, Nucl. Phys. A 928, 234 (2014).
[45] Jun Xu, Taesoo Song, Che Ming Ko, and Feng Li, Phys. Rev. Lett. 112, 012301 (2014).

[46] E. Retinskaya, M. Luzum, and J.-Y. Ollitrault, Phys.Rev. C 89, 014902 (2014).

[47] E. Retinskaya, M. Luzum, and J.-Y. Ollitrault, Nucl. Phys. A 926, 152 (2014).

[48] C. Lang and N. Borghini, Eur.Phys.J. C 74, 2955 (2014).

[49] J. Adams et al., (STAR Collaboration), Phys. Rev. Lett. 92, 062301 (2004).

[50] A. Adare et al., (PHENIX Collaboration), Phys. Rev. Lett. 105, 062301 (2010).

[51] D. Molnar and S. A. Voloshin, Phys. Rev. Lett. 91, 092301 (2003).

[52] T. Hirano and Y. Nara, Phys. Rev. C 69, 034908 (2004).

[53] H. van Hecke et al., Phys. Rev. Lett. 81, 5764 (1998).